Aalborg Universitet

AALBORG UNIVERSITY

DENMARK

Distributed Active Synchronization Strategy for Microgrid Seamless Reconnection to the Grid under Unbalance and Harmonic Distortion

Tang, Fen; Guerrero, Josep M.; Vasquez, Juan Carlos; Wu, Dan; Meng, Lexuan

Distributed Active Synchronization Strategy for Microgrid Seamless Reconnection to the Grid under Unbalance and Harmonic Distortion

Fen Tang, Josep M. Guerrero, *Fellow, IEEE*, Juan C. Vasquez, *Member, IEEE*, Dan Wu, and Lexuan Meng

Abstract–**Microgrids can operate in both grid-connected and islanded modes. In order to seamlessly transfer from islanded to grid-connected modes, it is necessary to synchronize microgrid voltage, frequency and phase to the main grid. However, since the microgrid is often based on power electronics converters, the synchronization process is quite different compared to the quasi-synchronism control in conventional power systems. Firstly, in order to address this concern, the microgrid synchronization criteria are derived. Based on these criteria, a novel distributed active synchronization strategy is proposed, which takes into account not only the fundamental component but also positive and negative sequences of the harmonic components. This way a seamless reconnection to the main grid can be performed. The proposed method is implemented in the secondary control level of a hierarchical control structure. Real-time hardware-in-the-loop results show the feasibility of the proposed technique.**

Index Terms—**Voltage harmonics, voltage unbalance, microgrid, synchronization, hierarchical control.**

NOMENCLATURE

C_{proj}	Cross product projection of $\mathbf{v}_m^{1+}$ and $\mathbf{v}_g^{1+}$ in the direction of the right-hand rule.
$\mathbf{F}$	Generic vector quantity.
F	Vector length of $\mathbf{F}$.
$G_V(s)$	Transfer function of the voltage control loop.
$G_I(s)$	Transfer function of the current control loop.
$G_{\mathrm{PWM}}(s)$	Transfer function of the pulse-width modulation block.
$G_{cc}(s)$	Voltage tracking transfer function.
$\mathbf{i_g}$	Measured grid current vector.
$\mathbf{i_L}$	Measured current vector of the filter-inductor.
$\mathbf{i_{Load}}$	Equivalent load current vector.
$\mathbf{i_o}$	Measured output current vector of the converter.
k_p	Proportional coefficient of active power droop controller.
k_q	Proportional coefficient of reactive power droop controller.
k_{sp}^h, k_{si}^h	Proportional and integral coefficients of PI controllers for DSC.
m	The total number of CCM-VSC units.
n	The total number of VCM-VSC units.
P_0	Active power before reconnection.
$P_{\mathrm{cal}}^{1+}, P^{1+}$	Unfiltered and filtered fundamental positive sequence active power.
$\Delta P^{1+}, \Delta Q^{1+}$	Synchronization active and reactive power resulted by the difference of fundamental positive sequence components.
$Q_{\mathrm{cal}}^{1+}, Q^{1+}$	Unfiltered and filtered fundamental positive sequence reactive power.
T_d	Communication delay.
$\mathbf{v_c}$	Measured voltage vector of the filter capacitor.
$\mathbf{v_g}$	Grid voltage vector at PCC.
$\mathbf{v_m}$	Microgrid voltage vector.
$\mathbf{v_{ref}}$	Reference voltage vector.
$\mathbf{v_s}$	Thévenin equivalent voltage source.
$\mathbf{v_{sync}^h}$	Output harmonic synchronization voltage vector of DSC.
$V_{\mathrm{sync\_dq}}^h$	Representation of $\mathbf{v_{sync}^h}$ in synchronous reference frame dq.
$\mathbf{v_{VSC}}$	Output voltage vector of the converter.
V^{1+}	Voltage amplitude of $\mathbf{v_{ref}^{1+}}$.
V^*	No-load voltage amplitude.
V_g	Voltage amplitude of $\mathbf{v_g}$.
V_m	Voltage amplitude of $\mathbf{v_m}$.
V_N	Nominal voltage amplitude.
V_{sync}	Output signal of amplitude synchronization block in FSC.
$\Delta \mathbf{v}$	Voltage vector difference of $\mathbf{v_m}$ and $\mathbf{v_g}$.
ΔV^{1+}	Amplitude difference between $\mathbf{v_m^{1+}}$ and $\mathbf{v_g^{1+}}$ at the instant of reconnection.
X	Designed value of z_o^{1+}.
$z_{cc}(s)$	Impedance transfer function of inner double closed-loops.
z_{cf}	Impedance of the filter capacitor.
z_f	Impedance of the filter inductor.
z_g	Grid impedance.
z_L	Equivalent impedance of the sum of grid-side inductor and feeder line impedances.
z_{Load}	Equivalent balanced linear load.
z_{non_Load}	Equivalent balanced nonlinear loads.
z_o	Thévenin equivalent source impedance.

Fen Tang is with National Active Distribution Network Technology Research Center (NANTEC), Beijing Jiaotong University, Beijing, P. R. China, 100044 (e-mail: ftang_nego@126.com).

Josep M. Guerrero, Juan C. Vasquez, Dan Wu, Lexuan Meng are with Department of Energy Technology, Aalborg University, 9220 Aalborg (e-mail: joz@et.aau.dk, juq@et.aau.dk, dwu@et.aau.dk, lme@et.aau.dk).

z_{op}	Shunt impedance of n Thévenin equivalent source impedances.
z_{t}	Equivalent total impedance, $z_{\text{t}} = z_{\text{op}} + z_{\text{g}}$.
$z_{\text{un\_Load}}$	Equivalent unbalanced linear load.
$z_{\text{vr}}(s)$	Transfer function of the virtual impedance loop.
$z_{\text{vreq}}(s)$	Equivalent virtual impedance.
ω	Angular frequency of $\mathbf{v}_{\text{ref}}^{1+}$.
ω^*	Rated angular frequency.
ω_{c}	Cut-off angular frequency of low pass filters.
ω_{g}	Angular frequency of $\mathbf{v}_{\text{g}}$.
ω_{m}	Angular frequency of $\mathbf{v}_{\text{m}}$.
ω_{sync}	Output signal of phase and frequency synchronization block in FSC.
$\Delta\omega^{1+}$	Angular frequency difference between $\mathbf{v}_{\text{m}}^{1+}$ and $\mathbf{v}_{\text{g}}^{1+}$ at the instant of reconnection.
θ_{f}	Angle between $\mathbf{F}$ and a axis.
θ_{g0}	Initial angles of $\mathbf{v}_{\text{g}}$.
θ_{m0}	Initial angles of $\mathbf{v}_{\text{m}}$.
$\Delta\theta_0^{1+}$	Initial angle difference between $\mathbf{v}_{\text{m}}^{1+}$ and $\mathbf{v}_{\text{g}}^{1+}$ at the instant of reconnection.

- *Superscripts*

1+	Fundamental positive sequence component.
h	Fundamental negative sequence and low-order harmonic components.

- *Subscripts*

a, b, c	Three phase natural reference frame quantities.
d, q	Two phase synchronization reference frame quantities.
k	Index of VCM-VSC units, $k=1,2,...,n$.
ref	Reference quantities.
α, β	Two phase stationary reference frame quantities.

- *Abbreviations*

CCM	Current-controlled mode.
DR	Distributed resources.
DG	Distributed generation.
DS	Distributed storage.
DSC	Distortion synchronization control, referring to the synchronization control of fundamental negative sequence and low-order harmonic components.
FSC	Fundamental synchronization control, referring to the synchronization control of fundamental positive sequence components.
HiL	Hardware-in-the-loop.
IHD	Individual harmonic distortion.
PCC	Point of common coupling.
PI	Proportional integral.
PLL	Phase-locked loop.
PWM	Pulse-width modulation.
STS	Static transfer switch.
THD	Total harmonic distortion.
UF	Unbalance factor.
VSC	Voltage source converter.
VCM	Voltage-controlled mode.

I. INTRODUCTION

NOWADAYS, the microgrid concept is attracting much attention since it is considered as a promising way to integrate distributed resources (DRs). A microgrid can be defined as a local distributed electrical network consisting of DR units and dispersed loads, which can operate in both grid-connected and islanded modes [1]. In order to guarantee uninterruptible and reliable power supply, a smooth transition from islanded to grid-connected modes is required. To achieve this goal, it is necessary to synchronize microgrid voltage, frequency and phase to the main grid.

Due to the introduction of various DRs and power electronics equipment such as converters, the synchronization process of a microgrid is quite different compared to the quasi-synchronism control in conventional rotating machine-based power systems. The following issues should be reconsidered.

Compared to conventional power systems, power-electronics-based microgrids usually present fast dynamic response, small inertia and low overload capability. Therefore, the synchronization criteria listed in the IEEE Std. 1547-2003 may not be proper for a power-electronics-based microgrid. In order to achieve a seamless reconnection of that kind of microgrids, the corresponding synchronization criteria should be first clarified.

Regarding microgrid reconnection issues, in [2] a method that uses virtual inductances is proposed in order to avoid active synchronization. However, although this method protects generators against overcurrent, the voltage phase jump applied to loads cannot be avoided at the reconnection transient. In [3] and [4], several reconnection methods based on switching between control modes are proposed in order to ride through the transition between islanded and grid-connected modes. However, the system stability may be affected by using these methods. On the other hand, in most existing work microgrids and grids under balanced and harmonic-free conditions are always considered when applying synchronization control strategies, thus involving only the synchronization control of fundamental positive sequence components, named here as FSC. To achieve FSC, some methods which enforce microgrid voltage to directly track the main grid voltage are presented in [5] and [6]. However, those approaches are hardly feasible since they need to send time-domain signals such as phase angles, which may require high-speed communications. Alternatively, in [7] a unified controller is proposed, which includes amplitude and phase compensators, that drive local controllers of DR units. This way they can simultaneously shift up/down droop curves in order to get microgrid voltage synchronized with the main grid. In order to reduce the communication dependency, a central controller which uses a preset table is proposed in [8]. However, the logic table and decision maker algorithm is complex. In order to improve synchronization performance, some methods that synchronize frequency and phase in sequence are proposed in [9]-[12]. Nonetheless, overall synchronization time is prolonged due to the sub-period adjustments of phase and frequency. In addition, phase

regulation will also influence the frequency regulation, which needs to be considered in the design of frequency disturbance values or the switching sequence. Three control loops are respectively used for voltage, frequency and phase synchronizations, as presented in [13]. Although by using this method a seamless transfer can be achieved, the interaction between frequency and phase regulators may affect the accuracy of both variables in a practical case. Due to the geographical distribution of DRs, high-speed communication is hardly feasible compared to conventional power systems. Therefore, how to get a fast and stable synchronization without relying on high-speed communication systems is an issue.

During islanded mode, converter-dominated microgrids are sensitive to power quality disturbances, owing to the low short-circuit ratio and limited capacity. Although the voltage distortion i.e. total harmonic distortion (THD) <5%, unbalance factor <2%, is not enough to stress the synchronization process in conventional power systems, it may lead to instability, damage or deteriorate the power quality due to inrush harmonic current during the reconnection process. Consequently, this process under unbalanced and/or distorted voltage conditions should also take into account the synchronization of fundamental negative sequence and low-order harmonic components, named here as DSC. In this part, it is necessary to figure out whether DSC is needed and how to achieve DSC. In [14], although the use of DSC is suggested, the reason and how to implement it are not clarified.

To address the aforementioned three issues, this paper dedicates to the following aspects: i) microgrid synchronization criteria are derived; ii) an improved active FSC is proposed and iii) a simple active DSC method is proposed. Both FSC and DSC algorithms are implemented in the secondary control level of the microgrid hierarchical control structure. The paper aims to achieve a smooth transition from islanded to grid-connected modes when the grid or microgrid voltages are slightly distorted. The method is based on distorting the microgrid voltage to achieve a similar voltage waveform as in the grid side during the reconnection process. By using the proposed synchronization scheme, the inrush current during the reconnection is effectively reduced. The proposed method can be effectively applied when using hierarchically controlled microgrids [13], [15], [16].

This paper is organized as follows. In Section II, the system modeling during the transition process is derived. Afterwards, the transfer characteristics are analyzed in Section III. Based on the system modeling and transfer analysis, microgrid synchronization criteria are given. Furthermore, the new active FSC and DSC algorithms are proposed and discussed in Section IV. Real-time hardware-in-the-loop (HiL) scenario studies are carried out in Section V. Section VI gives the conclusion.

II. MICROGRID MODELING DURING TRANSITION FROM ISLANDED TO GRID-CONNECTED MODES

This Section firstly gives a brief introduction of microgrid system configuration and primary control structure of
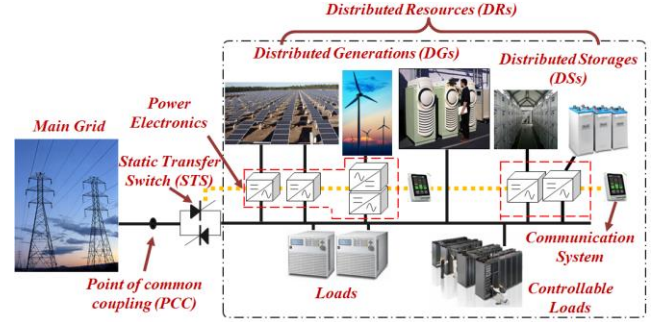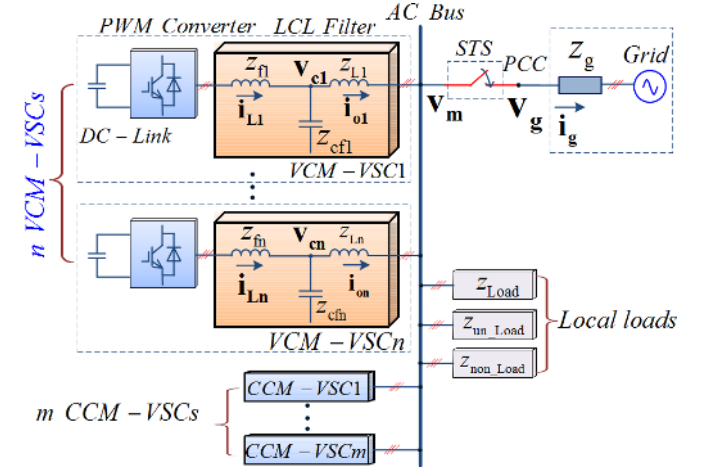

Fig. 1. A microgrid configuration example.

Fig. 2. Simplified structure of a microgrid.

converters. Afterwards microgrid modeling during the transition process is derived, which consists of two parts: i) modeling of fundamental positive sequence component and ii) modeling of fundamental negative sequence and harmonic components.

A. Microgrid System Configuration

Fig. 1 shows a microgrid configuration example [1]. A voltage source converter (VSC) is usually employed as an interface between a DR unit and a microgrid. Two types of control strategies can be used to operate VSCs: current-controlled mode (CCM) and voltage-controlled mode (VCM) [17]. CCM-VSC units are normally used to interface renewable energy such as wind turbines and photovoltaic systems. For these units the transition from islanded to grid-connected modes is not a significant issue because the local phase-locked loop (PLL) will synchronize converters with the grid (main grid or microgrid). However, unlike CCM-VSC units, VCM-VSC units are usually used for distributed storages (DSs) to provide power balance and voltage support in islanded mode, and at the same time they can act as distributed actuators for active FSC and DSC algorithms.

Based on the above analysis, the simplified structure of a microgrid based on *n* VCM-VSCs and *m* CCM-VSCs is shown in Fig. 2.

In this paper, vector analysis is used [18], [19]. For a generic vector quantity **F**, its projection components on three phase natural reference frame *abc* and two phase stationary reference frame *αβ* are respectively denoted by subscripts (*a*, *b*, *c*) and (*α*, *β*). By defining *F* as vector length and *θ*f as the

angle between **F** and *a* axis, the relationship can be expressed as

$$\mathbf{F} = 2(f_a + af_b + a^2 f_c)/3 = f_\alpha + jf_\beta = Fe^{j\theta_f} \quad (1)$$

where $a=e^{j2\pi/3}$.

B. Primary Control Structure of VCM-VSC Units

The primary control structure for VCM-VSC units is shown in Fig. 3, which mainly includes a droop control block, a virtual impedance loop and inner double closed-loops [13]. There are two types of input signals: i) three measured vector signals $\mathbf{v_c}$, $\mathbf{i_o}$ and $\mathbf{i_L}$ (brown color) from the VCM-VSC unit; ii) three synchronization signals ω_{sync}, V_{sync} and $V_{sync\_dq}^h$ (blue color) are received from secondary control level through the low-bandwidth communication link. $V_{sync\_dq}^h$ is the representation of $\mathbf{v}_{sync}^h$ in synchronous reference frame dq, which will be transformed into corresponding components in the two phase stationary reference frame $\alpha\beta$ as shown in Fig. 3. Notice that ω_{sync} and V_{sync} are used by the FSC; $\mathbf{v}_{sync}^h$ is used by the DSC. These three signals will be discussed in Section IV.

As shown in Fig. 3, the fundamental positive sequence power is first calculated and fed into the droop control block to generate the fundamental positive sequence component $\mathbf{v}_{ref}^{1+}$ of reference voltage vector. Thus, the angular frequency ω, amplitude V^{1+}, and phase angle θ_{ref}^{1+} of $\mathbf{v}_{ref}^{1+}$ can be expressed as [13]

$$\begin{cases} \omega = \omega^* + \omega_{sync} - k_p P^{1+} = \omega^* + \omega_{sync} - k_p P_{cal}^{1+}\omega_c/(s+\omega_c) \\ V^{1+} = V^* + V_{sync} - k_q Q^{1+} = V^* + V_{sync} - k_q Q_{cal}^{1+}\omega_c/(s+\omega_c) \quad (2) \\ \theta_{ref}^{1+} = \omega/s \end{cases}$$

Combined with the harmonic synchronization voltage vector $\mathbf{v}_{sync}^h$, the reference voltage vector $\mathbf{v_{ref}}$ is obtained as

$$\mathbf{v_{ref}} = \mathbf{v}_{ref}^{1+} + \mathbf{v}_{sync}^h \quad (3)$$

Regarding inner double closed-loops, the detailed design procedure can be found in [13] and [16]. By using the inner double closed-loops, $\mathbf{v_{VSC}}$, $\mathbf{v_C}$ and $\mathbf{i_L}$ can be derived as

$$\begin{cases} \mathbf{v_{VSC}} = (G_V(s)(\mathbf{v_{ref}} - \mathbf{v_{vr}} - \mathbf{v_c}) - \mathbf{i_L})G_I(s)G_{PWM}(s) \\ \mathbf{v_C} = (\mathbf{i_L} - \mathbf{i_o})z_{cf}(s) \quad (4) \\ \mathbf{i_L} = (\mathbf{v_{VSC}} - \mathbf{v_C})/z_f(s) \end{cases}$$

Eliminating $\mathbf{v_{VSC}}$ and $\mathbf{i_L}$, $\mathbf{v_c}$ can be rewritten as

$$\begin{aligned} \mathbf{v_c} &= G_{cc}(s)(\mathbf{v_{ref}} - \mathbf{v_{vr}}) - z_{cc}(s)\mathbf{i_o} \\ &= G_{cc}(s)\mathbf{v_{ref}} - (z_{cc}(s) + G_{cc}(s)z_{vr}(s))\mathbf{i_o} \quad (5) \\ &= G_{cc}(s)\mathbf{v_{ref}} - (z_{cc}(s) + z_{vreq}(s))\mathbf{i_o} \end{aligned}$$

where

$$\begin{cases} G_{cc}(s) = \dfrac{G_V(s)G_I(s)G_{PWM}(s)}{\dfrac{z_f(s)}{z_{cf}(s)} + G_V(s)G_I(s)G_{PWM}(s) + \dfrac{G_I(s)G_{PWM}(s)}{z_{cf}(s)} + 1} \\[4mm] z_{cc}(s) = \dfrac{z_f(s) + G_I(s)G_{PWM}(s)}{\dfrac{z_f(s)}{z_{cf}(s)} + G_V(s)G_I(s)G_{PWM}(s) + \dfrac{G_I(s)G_{PWM}(s)}{z_{cf}(s)} + 1} \end{cases}$$

Thus based on (5), microgrid voltage vector $\mathbf{v_m}$ can be described as

$$\begin{aligned} \mathbf{v_m} &= \mathbf{v_c} - z_L(s)\mathbf{i_o} \\ &= G_{cc}(s)\mathbf{v_{ref}} - (z_{cc}(s) + z_{vreq}(s) + z_L(s))\mathbf{i_o} \end{aligned} \quad (6)$$
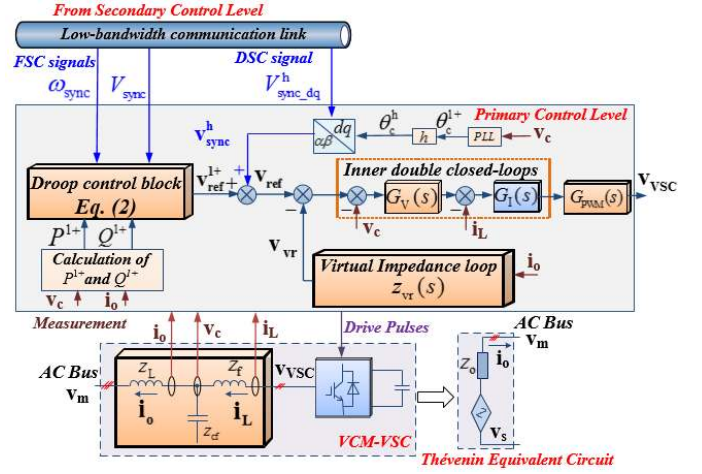

Fig. 3. Primary control structure for VCM-VSC units.

According to the Thévenin theorem, each VCM-VSC can be represented as equivalent voltage source $\mathbf{v_s}$ in series connection with equivalent source impedance z_o, as shown in Fig. 3. Therefore $\mathbf{v_m}$ can be rewritten as

$$\mathbf{v_m} = \mathbf{v_s} - z_o(s)\mathbf{i_o} \quad (7)$$

Comparing (6) and (7), $\mathbf{v_s}$ and $z_o(s)$ can be described as

$$\mathbf{v_s} = G_{cc}(s)\mathbf{v_{ref}} = G_{cc}(s)(\mathbf{v}_{ref}^{1+}(s) + \mathbf{v}_{sync}^h(s)) \quad (8)$$

$$z_o(s) = z_{cc}(s) + z_{vreq}(s) + z_L(s) \quad (9)$$

where $z_o(s)$ is composed of three terms: i) impedance $z_{cc}(s)$ due to inner double closed-loops; ii) equivalent virtual impedance $z_{vreq}(s) = G_{cc}(s)z_{vr}(s)$; and iii) $z_L(s)$.

Notice that due to the much higher bandwidth of inner closed-loops compared to the dominant harmonic frequencies, $G_{cc}(s)$ and $z_{cc}(s)$ are respectively around 1 and 0 at these frequencies [13], [16]. Therefore, by using virtual impedance loop, the characteristic of $z_o(s)$ can be reshaped, next to the desired value $z_{vr}(s)$. To get a good current-sharing, $z_{vr}(s)$ is usually set to a large, where $z_L(s)$ can be neglected. In this sense, $z_o(s)$ is approximately equal to $z_{vr}(s)$ at the frequency of interest. The detailed design procedure for the virtual impedance loop can be referred to [16] and [20]. In this paper, fundamental positive sequence impedance z_o^{1+} is designed to be mainly inductive and it can be simply represented by jX.

C. Microgrid Modeling During the Transition Process

Based on the above analysis, the influence of $\Delta\mathbf{v}$ on the system response can be studied by analyzing the simplified electrical network circuit as shown in Fig. 4(a), where each VCM-VSC unit is represented as $\mathbf{v_s}$ in series connection with z_o; $\mathbf{i_{Load}}$ is the equivalent current source to perform the loads including all the actual loads and CCM-VSC units.

According to the superposition theorem, the system response can be divided into two parts: i) response of fundamental positive sequence component, where the variables are denoted by superscript 1+; and ii) response of fundamental negative sequence and low-order harmonic components, where the variables are denoted by superscript h. Their equivalent circuits are respectively shown in Fig. 4(b) and Fig. 4(c).

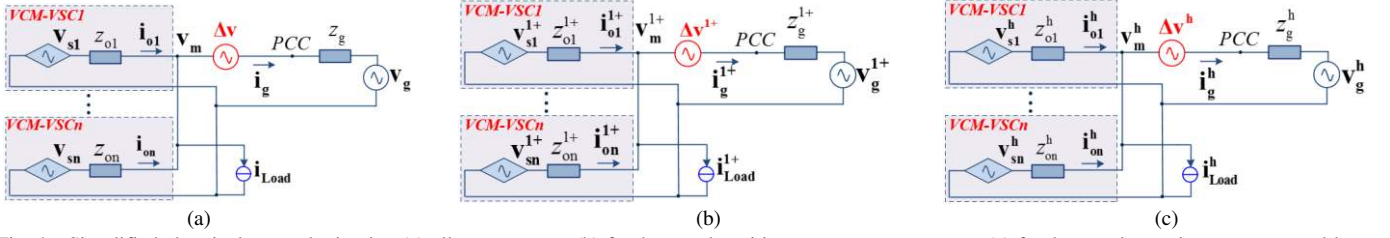### i) Modeling of Fundamental Positive Sequence Component

(a)

(b)

(c)

Fig. 4. Simplified electrical network circuits. (a) all components; (b) fundamental positive sequence component; (c) fundamental negative sequence and low-order harmonic components.

Based on (8), (9) and the analysis done in Subsection II. B, the fundamental positive sequence Thévenin equivalent voltage source $\mathbf{v_s^{1+}}$ and source impedance z_o^{1+} in Fig. 4(b) can be derived as

$$\begin{cases} \mathbf{v_s^{1+}} \approx \mathbf{v_{ref}^{1+}} \\ z_o^{1+} \approx jX \end{cases} \tag{10}$$

Let V_s^{1+} and θ_s^{1+} be the amplitude and angle of $\mathbf{v_s^{1+}}$, while V_m^{1+} and θ_m^{1+} be the amplitude and angle of $\mathbf{v_m^{1+}}$, respectively. For each VCM-VSC unit as shown in Fig. 4(b), fundamental positive sequence active power and reactive power can be expressed as

$$\begin{cases} P^{1+} = \dfrac{3}{2} \dfrac{V_s^{1+}V_m^{1+}}{X} \sin(\theta_s^{1+} - \theta_m^{1+}) \\ Q^{1+} = \dfrac{3}{2} \dfrac{V_s^{1+}V_m^{1+}\cos(\theta_s^{1+} - \theta_m^{1+}) - (V_m^{1+})^2}{X} \end{cases} \tag{11}$$

Since the difference between θ_s^{1+} and θ_m^{1+} is usually small, the following approximations can be obtained.

$$\begin{cases} \sin(\theta_s^{1+} - \theta_m^{1+}) \approx \theta_s^{1+} - \theta_m^{1+} \\ \cos(\theta_s^{1+} - \theta_m^{1+}) \approx 1 - (\theta_s^{1+} - \theta_m^{1+})^2/2 \end{cases} \tag{12}$$

Thus (11) can be rewritten as

$$\begin{cases} P^{1+} \approx \dfrac{3}{2} \dfrac{V_s^{1+}V_m^{1+}}{X} (\theta_s^{1+} - \theta_m^{1+}) \\ Q^{1+} \approx \dfrac{3}{2} \dfrac{V_m^{1+}}{X} (V_s^{1+} - V_m^{1+}) - \dfrac{3}{4} \dfrac{V_s^{1+}V_m^{1+}(\theta_s^{1+} - \theta_m^{1+})^2}{X} \\ \approx \dfrac{3}{2} \dfrac{V_m^{1+}}{X} (V_s^{1+} - V_m^{1+}) - \dfrac{3}{4} \dfrac{V_s^{1+}V_m^{1+}(2P^{1+}X/(3V_s^{1+}V_m^{1+}))^2}{X} \\ \approx \dfrac{3}{2} \dfrac{V_m^{1+}}{X} (V_s^{1+} - V_m^{1+}) - \dfrac{X(P^{1+})^2}{3V_s^{1+}V_m^{1+}} \end{cases} \tag{13}$$

Based on (2) and (13), the equivalent fundamental positive sequence power control diagrams can be described as shown in Fig. 5, where red dashed boxes are taken effect during reconnection process.

ii) Modeling of Fundamental Negative Sequence and Harmonic Components

Based on (8), (9) and the analysis done in Subsection II. B, the harmonic Thévenin equivalent voltage source $\mathbf{v_s^h}$ and source impedance z_o^h in Fig. 4(c) can be given as

$$\begin{cases} \mathbf{v_s^h} \approx \mathbf{v_{sync}^h} \\ z_o^h \approx z_{vr}^h \end{cases} \tag{14}$$

If $\mathbf{v_{sync}^h}$ is broadcasted, all the $\mathbf{v_{sk}^h}(k=1,2,..n)$ can be the same. In islanded mode, the STS at PCC is open. Thus, only the independent sources $\mathbf{v_s^h}$ and $\mathbf{i_{Load}^h}$ are considered. According to
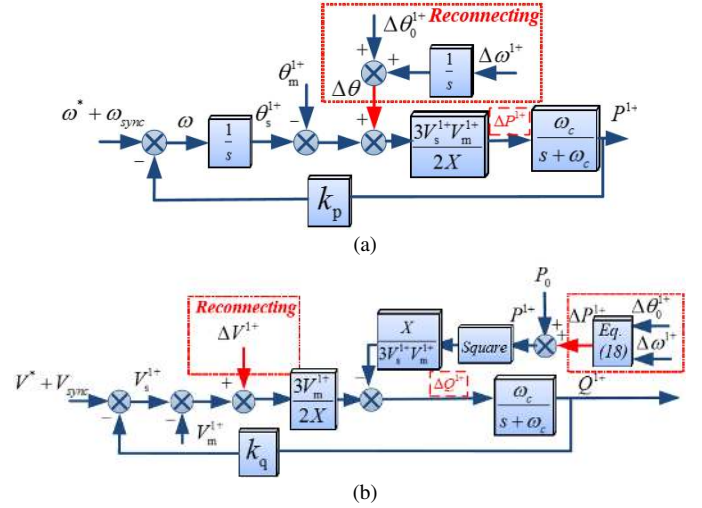

(a)

(b)

Fig. 5. Equivalent fundamental positive sequence power control diagrams. (a) active power; (b) reactive power.

superposition theorem, $\mathbf{v_m^h}$ and $\mathbf{i_o^h}$ can be calculated as

$$\begin{cases} \mathbf{v_m^h} = \mathbf{v_s^h} - \mathbf{i_{Load}^h} z_{op}^h \\ \mathbf{i_o^h} = (\mathbf{v_s^h} - \mathbf{v_m^h})/z_o^h = \mathbf{i_{Load}^h} z_{op}^h/z_o^h \end{cases} \tag{15}$$

where $z_{op}^h = 1/\sum_{i=1}^{n}(1/z_{oi}^h)$.

At the instant of closing STS, $\mathbf{i_g^h}$ can be inferred as

$$\mathbf{i_g^h} = \Delta\mathbf{v^h}/z_t^h \tag{16}$$

where the equivalent total impedance $z_t^h = z_{op}^h + z_g^h$.

III. ANALYSIS OF THE TRANSITION FROM ISLANDED TO GRID-CONNECTED MODES

Based on models derived in Section II, analysis of the transition from islanded to grid-connected modes is presented in this Section, which consists of two parts: i) effect of the fundamental positive sequence component; and ii) effect of the fundamental negative sequence and harmonic components. Based on i), microgrid synchronization criteria are presented. Based on ii), DSC is needed to achieve a smooth transition.

A. Effect of the Fundamental Positive Sequence Component

At the moment of closing STS, step inputs $\Delta\omega^{1+}$, ΔV^{1+} and $\Delta\theta_0^{1+}$ are applied. Thus ΔP^{1+} and ΔQ^{1+} can be derived from Fig. 5 as

$$\begin{cases} \Delta P^{1+}(s) = \dfrac{k_\theta(s+\omega_c)}{\omega_c(s^2+\omega_c s+k_p k_\theta)}\left(\dfrac{\Delta\omega^{1+}}{s}+\Delta\theta_0^{1+}\right) \\ \Delta Q^{1+}(s) \approx \dfrac{k_V(s+\omega_c)}{\omega_c(s+\omega_c+k_q k_V)}\dfrac{\Delta V^{1+}}{s}+k_{PQ}\Delta P^{1+}(s) \end{cases} \tag{17}$$

where $k_{PQ}=-2XP_0/3/V_s^{1+}/V_m^{1+}$; $k_{\theta}=3\omega_c V_s^{1+} V_m^{1+}/2X$; $k_V=3\omega_c V_m^{1+}/2/X$.

Since usually $k_p k_{\theta}>>(\omega_c^2)/4$, based on (17), step responses can be expressed as

$$\begin{cases} \Delta P^{1+}(t) = G_{P\theta}\Delta\theta_0^{1+} + G_{P\omega}\Delta\omega^{1+} \\ \Delta Q^{1+}(t) = G_{QV}\Delta V^{1+} + k_{PQ}G_{P\theta}\Delta\theta_0^{1+} + k_{PQ}G_{P\omega}\Delta\omega^{1+} \end{cases} \quad (18)$$

where

$$\begin{cases} G_{P\omega} = \dfrac{1}{k_p} - \dfrac{k_{\theta}\sin(bt+\gamma_1)}{\omega_c b}e^{-\frac{\omega_c t}{2}} \approx \dfrac{1}{k_p} - \dfrac{\sin(bt+\gamma_1)}{\omega_c}\sqrt{\dfrac{k_{\theta}}{k_p}}e^{-\frac{\omega_c t}{2}} \\ G_{P\theta} = \dfrac{k_{\theta}\sqrt{k_p k_{\theta}}\sin(bt+\gamma_2)}{\omega_c b}e^{-\frac{\omega_c t}{2}} \approx \dfrac{k_{\theta}\sin(bt+\gamma_2)}{\omega_c}e^{-\frac{\omega_c t}{2}} \\ G_{QV} = \dfrac{k_V}{k_q k_V + \omega_c}\left[1+\dfrac{k_V k_q}{\omega_c}e^{-(k_q k_V+\omega_c)t}\right] \end{cases} \quad (19)$$

being $b=(k_p k_{\theta}-\omega_c^2/4)^{0.5}$; $\gamma_1=\tan^{-1}(-b\omega_c/(k_p k_{\theta}-\omega_c^2/2))$; and $\gamma_2=\tan^{-1}(2b/\omega_c)$.

The grid current vector amplitude I_g^{1+} which is resulted from ΔP^{1+} and ΔQ^{1+} can be obtained as

$$I_g^{1+} = 2\sqrt{(\Delta P^{1+})^2 + (\Delta Q^{1+})^2}/(3V_g^{1+}) \quad (20)$$

It can be seen from (18) that ΔP^{1+} is mainly influenced by $\Delta\omega^{1+}$ and $\Delta\theta_0^{1+}$. Since usually $k_{PQ}<<1$, if amplitude synchronization is achieved at the instant of reconnection, then $\Delta Q^{1+}<<\Delta P^{1+}$. Therefore, it can be observed from (20) that I_g^{1+} is mainly influenced by ΔP^{1+}.

The synchronization criteria listed in the IEEE Std 1547-2003 are shown in Table I. Using the synchronization parameter limits for less than 500kVA in Table I, and assuming $P_0=1$kW, step responses with different system parameters are discussed in four cases as shown in Table II.

- *Case A1 : ΔP^{1+} and ΔQ^{1+} with different X*

The step responses for different X are shown in Fig. 6. From these results, the following conclusions can be achieved.

i) Since $k_q k_V>>\omega_c$, it can be derived from (19) that the attenuation rate of G_{QV} is much higher than $G_{P\omega}$ and $G_{P\theta}$. Thus, it can be observed that the attenuation rates of curves in Fig. 6(e) are much higher than those in Figs. 6(a) ~(d).

ii) Since $k_{PQ}<<1$, comparing Fig. 6 (a) with Fig. 6(c), Fig. 6 (b) with Fig. 6(d), for the same $\Delta\omega^{1+}$ and $\Delta\theta_0^{1+}$, it can be seen that $\Delta Q^{1+}<<\Delta P^{1+}$.

iii) Comparing Figs. 6 (a)~(e), the synchronization active power resulted from phase angle difference is the largest. Based on (20), I_g^{1+} is mainly influenced by ΔP^{1+}. Therefore, it can be derived from (19) that initial oscillation amplitude of grid current is reduced when increasing X. However, X barely has effect on the steady-state grid current as shown in Fig. 6(f).

- *Case A2~A4 : I_g^{1+} with different k_p, k_q and ω_c*

The step responses I_g^{1+} for different k_p, k_q and ω_c are shown in Fig. 7. As illustrated in *Case A1*, I_g^{1+} is mainly influenced by ΔP^{1+}. Therefore, based on (19), initial oscillation amplitude of grid current remains almost unchanged with the variations of k_p, k_q and ω_c, as shown in Fig. 7. It can be also observed that the steady-state grid current is mainly influenced by k_p.

(a) $G_{P\omega}\Delta\omega^{1+}$ in (18)   (b) $G_{P\theta}\Delta\theta_0^{1+}$ in (18)

(c) $k_{PQ}G_{P\omega}\Delta\omega^{1+}$ in (18)   (d) $k_{PQ}G_{P\theta}\Delta\theta_0^{1+}$ in (18)

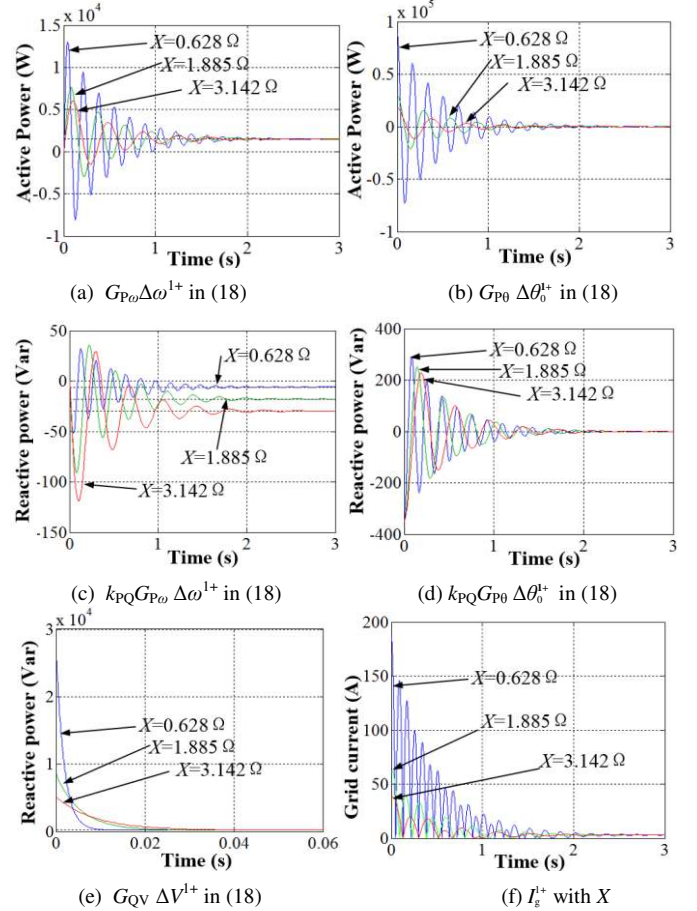(e) $G_{QV}\Delta V^{1+}$ in (18)   (f) I_g^{1+} with X

Fig. 6.   Case A1: Step responses for *different X*.

TABLE I
IEEE STD 1547-2003 SYNCHRONIZATION PARAMETER LIMITS

Aggregate rating of DR units (kVA)	Frequency difference (Hz)	Voltage difference (%)	Phase angle difference (°)
0-500	0.3	10	20
>500-1500	0.2	5	15
>1500-10 000	0.1	3	10

TABLE II
SYSTEM PARAMETERS IN DIFFERENT CASES

	ω_c (rad/s)	k_p (rad·s^{-1}/W)	k_q (V/Var)	X (Ω)
Case A1	4.4	0.00126	0.16	0.63~3.14
Case A2	4.4	0.00063~0.00314	0.16	1.257
Case A3	4.4	0.00126	0.13~0.19	1.257
Case A4	1.9~6.9	0.00126	0.16	1.257

Based on (19), Figs. 6 and 7, by reducing phase angle difference $\Delta\theta_0^{1+}$ or increasing virtual impedance, transient grid current amplitude can be reduced. While by reducing $\Delta\omega^{1+}$ and ΔV^{1+} or increasing k_p, steady-state grid current can be decreased. However, large virtual impedance will deteriorate the power quality of voltage. Based on (2), k_p is usually restricted by the maximum frequency deviation. Besides redesigning virtual impedance and k_p, another effective way to achieve a smooth reconnection is to reduce Δv^{1+}.

In the case study, k_p, k_q, and ω_c are chosen to be the same as in *Case A1* and X is selected as 1.257 Ω. If transient and steady-state grid current amplitudes are respectively limited within 5% and 1% of nominal current, then based on (19), the
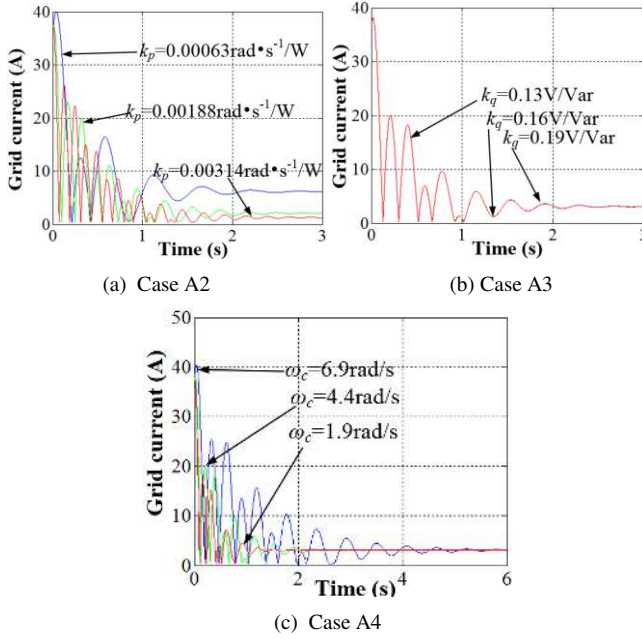
(a) Case A2   (b) Case A3

(c) Case A4

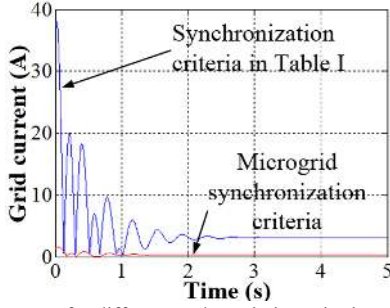Fig. 7. Case A2~A4: Step responses for different k_p, k_q and ω_c.

Fig. 8. Step responses for different sychronziation criteria.

synchronization parameter limits $\Delta\omega^{1+}$, ΔV^{1+} and $\Delta\theta_0^{1+}$ should satisfy the following equations.

$$\begin{cases} \Delta\omega^{1+} \leq 0.2\,\text{rad/s} \\ \Delta V^{1+} \leq 0.01 V_N \\ \Delta\theta_0^{1+} \leq 0.57° \end{cases} \quad (21)$$

These three conditions are named here as *microgrid synchronization criteria*. The step responses for different synchronization criteria are shown in Fig. 8. It can be observed that I_g^{1+} can be largely reduced with *microgrid synchronization criteria*.

The above analysis provides the principle of setting microgrid synchronization criteria. Given k_p, k_q, ω_c and grid current limits, based on (19), synchronization criteria can be derived.

B. Effect of the Fundamental Negative Sequence and Harmonic Components

If the reconnection is enabled without using DSC, then $\mathbf{v_s^h}$ =0. Based on (15), in islanded mode, $\mathbf{v_m^h}$ can be written as

$$\mathbf{v_m^h} = -\mathbf{i_{Load}^h} z_{op}^h \quad (22)$$

Thus at the instant of reconnection, $\Delta\mathbf{v^h}$ can be obtained as

$$\Delta\mathbf{v^h} = -\mathbf{i_{Load}^h} z_{op}^h - \mathbf{v_g^h} \quad (23)$$

The worst case is that $\mathbf{v_m^h}$ and $\mathbf{v_g^h}$ are both at the limits of requirements and out of phase by 180 degrees. If the limits are the same for $\mathbf{v_m^h}$ and $\mathbf{v_g^h}$, $\Delta\mathbf{v^h}$ is almost $2\mathbf{i_{Load}^h}z_{op}^h$. Also in this case, the microgrid is supplying maximum nonlinear loads. If z_g=0, then twice harmonic current will flow though the STS according to (16) and (23), which will deteriorate the power quality of grid. Also, it can be obtained that the phase of $\mathbf{i_o^h}$ will be reversed, which may lead to instability.

If $\mathbf{i_{Load}^h}$=0 and z_g=0, based on (16) and (23), grid current will be rewritten as

$$\mathbf{i_g^h} = -\mathbf{v_g^h} / z_{op}^h \quad (24)$$

Based on (22), z_{op}^h is expected to be as small as possible for power quality purposes. However, according to (24) and with respect to current sharing, z_{op}^h is desired to be as large as possible. This trade-off makes virtual impedance hard to design. Moreover, z_{op}^h is restricted by the smallest impedance. Besides virtual impedance methods, another effective way to achieve a smooth reconnection is to reduce $\Delta\mathbf{v^h}$, which will be discussed in Section IV. In this way, power quality can be ensured by the secondary control level, while transient response is guaranteed by DSC. In this sense, virtual impedance can be used for current-sharing, oscillation-damping, and active and reactive power decoupling purposes, thus resulting in an easier and systematic design procedure.

If DSC is used, the control objective during the synchronization process is to track $\mathbf{v_g^h}$. If $\mathbf{v_{syn}^h}$ is given as (25), then $\mathbf{v_m^h}$ will be the same as $\mathbf{v_g^h}$ according to (14) and (15).

$$\mathbf{v_{syn}^h} = \mathbf{i_{Load}^h} z_{op}^h + \mathbf{v_g^h} \quad (25)$$

Notice that in islanded mode, based on (15), $\mathbf{i_o^h}$ is almost the same as that when $\mathbf{v_s^h}$=0. In addition, inrush harmonic current flowing though the STS can be avoided at the instant of reconnection.

IV. PROPOSED SYNCHRONIZATION ALGORITHM

In this Section, a distributed active synchronization algorithm is proposed to achieve a smooth reconnection even under distorted and unbalanced voltage conditions. It takes into account not only the fundamental component but also positive and negative sequences of the harmonic components.

In islanded mode, microgrid frequency and voltage are determined by all the DRs and loads. Thus synchronization control involves a coordinated control of all the controllable distributed units, which is suitable by applying secondary control level in a hierarchical control structure [15]. Therefore, the proposed method is implemented in the secondary control level, which consists of a synchronization check block, active FSC and DSC, as shown in Fig. 9. There are two measured vector signals $\mathbf{v_m}$ and $\mathbf{v_g}$ (brown color), where $(V_m, \omega_m, \theta_{m0})$ and $(V_g, \omega_g, \theta_{g0})$ are respectively amplitudes, frequencies, and initial angles of $\mathbf{v_m}$ and $\mathbf{v_g}$. Three output signals ω_{sync}, V_{sync} and $V_{sync\_dq}^h$ (blue color) are broadcasted to primary controllers by means of low-bandwidth communication link.
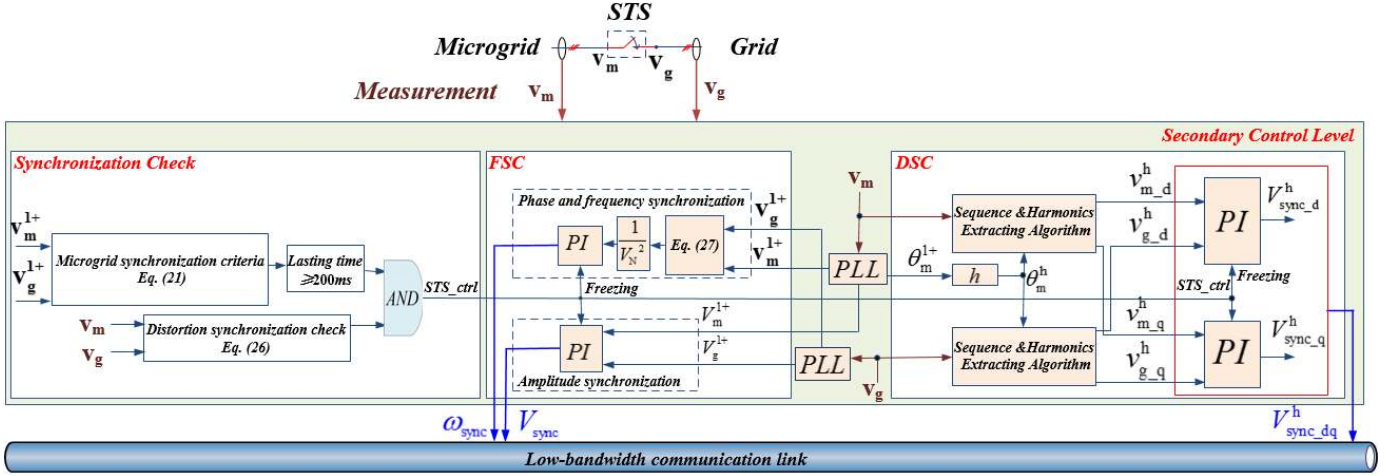
Fig. 9.   Proposed active synchronization control.

A. Synchronization Check

Based on the analysis in Section III, the synchronization check includes i) *microgrid synchronization criteria*. To ensure a stable operation and avoid disturbances, all the three quantities need to be within the limits as shown in (21) for a long time such as ten fundamental periods; and ii) *distortion synchronization check*, which requires $\Delta \mathbf{v^h}$ within a threshold during the reconnection mode. Besides the parameter limits, it is also necessary to make sure that the power quality of microgrid and main grid is within acceptable limits before closing the STS. Different standards [21]-[26] present different specific requirements. In this paper, regarding voltage harmonics, IEEE Std 519-1992 is considered: voltage individual harmonic distortion (IHD) <3% and voltage total harmonic distortion (THD) <5%, while the maximum allowable voltage unbalance factor (UF) is 2%. Therefore, either $\mathbf{v_m}$ in islanded mode or $\mathbf{v_m}$ and $\mathbf{v_g}$ in reconnection mode are needed to meet the abovementioned requirements. Accordingly, the distortion synchronization check can be described as

$$\begin{cases} UF_{vm}, UF_{vg} \le 2\% \\ IHD_{vm}, IHD_{vm} \le 3\% \\ THD_{vm}, THD_{vm} \le 5\% \\ \left| \Delta \mathbf{v^h} \right| \le 0.2\% V_N \qquad h = -1, \pm 3, \pm 5, \pm 7, \pm 11, \pm 13 \end{cases} \quad (26)$$

where a hysteresis band for $\Delta \mathbf{v^h}$ is utilized in order to avoid chattering phenomenon.

It needs to be clarified that different harmonic components in (26) can be considered depending on the application. For example, in case of supplying balanced nonlinear loads (e.g. full-bridge diode rectifier), harmonic components (h=−5,+7,−11,+13) are considered. But in case of unbalanced linear loads, only the fundamental negative sequence component (h= −1) needs to be included. In the more general case, linear/nonlinear balanced/unbalanced loads, all the positive and negative sequence components for every harmonic (h= −1, ±3, ±5, ±7, ±11, ±13) should be taken into count. Generally, due to the limited control bandwidth, only low-order harmonic components (h≤13) are considered. Notice that computational

complexity is acceptable and comparable to the harmonic compensator block of a single converter [27], [28].

B. Active FSC

The cross product projection C_{proj} of $\mathbf{v_m^{1+}}$ and $\mathbf{v_g^{1+}}$ in the direction by right-hand rule can be expressed as

$$\begin{aligned} C_{proj} &= (\mathbf{v_m^{1+}} \times \mathbf{v_g^{1+}})_{proj} = V_m^{1+} V_g^{1+} \sin((\omega_g - \omega_m)t + \theta_{g0}^{1+} - \theta_{m0}^{1+}) \\ &= -v_{g\_\alpha}^{1+} v_{m\_\beta}^{1+} + v_{g\_\beta}^{1+} v_{m\_\alpha}^{1+} \end{aligned} \quad (27)$$

As shown in (27), C_{proj} can be simply calculated by using the components in $\alpha\beta$ reference frame. From (27), C_{proj} can reflect the angle difference between two vectors, which is composed of two parts: i) initial angle difference $\Delta\theta_0^{1+}$; and ii) angle difference resulted from angular frequency difference $\Delta\omega^{1+}$. Since voltage amplitudes are non-zero, C_{proj} can always zero only when both $\Delta\theta_0^{1+}$ and $\Delta\omega^{1+}$ are zero. Therefore, it can be used for frequency and phase synchronization. Furthermore, the maximum value of C_{proj} is the product of vector amplitudes, which are operated within a small range around nominal voltage when system meets reconnection requirements. Therefore, C_{proj} can be normalized by V_N^2, which can generalize the parameter design for different voltage levels.

Based on the above analysis, the structure of proposed FSC is shown in Fig. 9. It is composed of i) phase and frequency synchronization, and ii) amplitude synchronization, where proportional-integral (PI) controllers are used for both regulations. The tracking principle of frequency and phase control is similar as in a PLL. The projection C_{proj}, PI controller and primary controller can be seen respectively as phase detector, loop filter and voltage controlled oscillator of a PLL. Thus, the parameters of PI controllers can be designed according to the rules in [29], which have a tradeoff between speed and accuracy. The primary controllers shift up/down droop curves according to the received signals V_{sync} and ω_{sync}. Notice that the freezing signal *STS_ctrl* makes the output value of a PI controller to be fixed to the last value. This way it eliminates the PI action, while avoiding a transient overshoot.

Compared to active synchronization method presented in [13], the proposed method has the following features: i) only
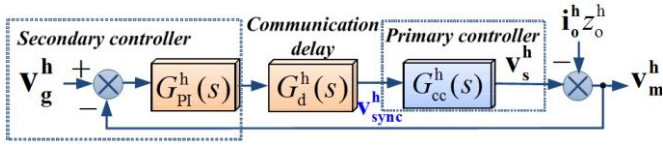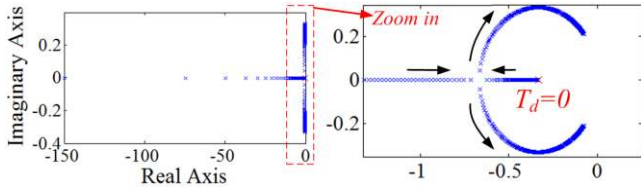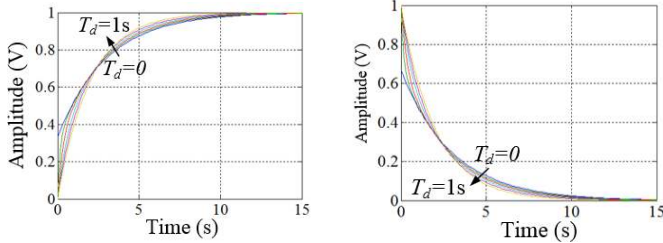
Fig. 10. Distortion synchronization control

Fig. 11. Root locus with T_d from 0 to 10s.

Fig. 12. Step responses. Left: Reference step; Right: Load step.

two regulators are needed; ii) it presents a typical PLL structure, so that the parameters can be easily designed; and iii) normalization with respect to the voltage is feasible, thus endowing further design simplicity.

C. Active DSC

The objective of this block is to actively limit $\Delta\mathbf{v}^h$ within a threshold during the reconnection process, as shown in Fig. 9. The basic idea of this method is to directly modify the references of these components in the primary controllers by using proper secondary control strategies, which is similar to the method verified in islanded mode [16]. The difference is the control strategy in the secondary control level. Since in islanded mode, it only needs to control these components within acceptable values, which is only related to the amplitudes. However, in reconnection mode, the control objective is to track $\mathbf{v}_g^h$, which is not only to match the amplitudes but also the phases. Moreover, the *Park transformation* is employed to overcome low-bandwidth communication limits. Thus fundamental negative sequence and harmonic components can be modulated as DC signals in the secondary controllers, and be demodulated back to harmonic signals in the primary controllers. As shown in Fig. 9, the fundamental negative sequence and low-order harmonic components in each synchronous reference frame are firstly extracted. Then the PI controller is used in each component to make microgrid track the corresponding grid component. In the secondary control level, $\mathbf{v}_g$ and $\mathbf{v}_m$ are measured, while in the primary control level $\mathbf{v}_c$ is sensed. When the DC signals are transformed back to the AC signals, the same reference angle needs to be used. However, due to the small difference in the fundamental angle between $\mathbf{v}_c$ and $\mathbf{v}_m$, θ_c^{1+} and θ_m^{1+} can be used as reference angles in the primary and secondary control levels respectively.
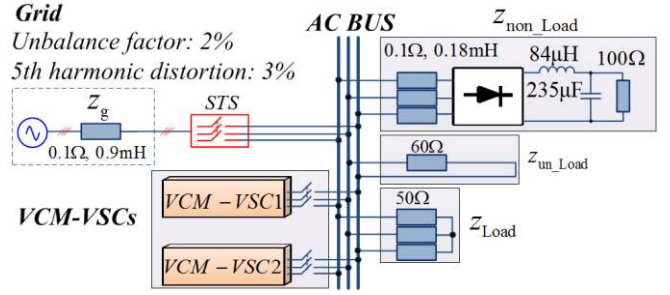
Based on the above analysis, Fig. 9 can be simplified into

Fig. 13. Real-time HiL configuration.

Fig. 10, where communication delay T_d is described by $G_d^h(s)$. Compared to the primary controllers, the secondary controllers usually have a slow control action. Hence dynamic responses of the primary controllers can be neglected when analyzing the performance of secondary controllers. Assuming the references can be real-time achieved $G_{cc}^h(s)=1$ and using first order approximation $G_d^h(s)=1/(T_d s+1)$, $\mathbf{v}_m^h$ can be given as

$$\mathbf{v}_m^h(s) = \frac{k_{sp}^h(s+k_{si}^h)\mathbf{v}_g^h(s)}{T_d s^2+(1+k_{sp}^h)s+k_{si}^h k_{sp}^h} - \frac{(T_d s^2+s)\mathbf{i}_o^h(s)z_o^h}{T_d s^2+(1+k_{sp}^h)s+k_{si}^h k_{sp}^h} \quad (28)$$

Using parameters in Table III, the root locus with T_d from 0 to 10s is illustrated in Fig. 11. It shows that the poles are always in the left-half plane, which means that the system is stable. Step responses of references and load disturbances are respectively shown in Fig. 12, which indicates that T_d has small influence on the steady-state performance. Fig. 12 also shows that the initial transient error is reduced when T_d decreases. Then by selecting proper PI controller parameters and T_d, DSC can be achieved. Since the secondary control level is slow in comparison to the primary control, the PI controller parameters can be the same for each harmonic component.

V. REAL-TIME HiL RESULTS

The proposed distributed active synchronization strategy is validated in a dSPACE 1006 based real-time HiL platform, with parameters shown in Table III. The HiL configuration is shown in Fig. 13. Without loss of generality, two VCM-VSCs are used in the setup and 5% parameter mismatch is used. In order to evaluate the performance of the proposed method, acceptable voltage distortion (e. g. 2% unbalanced factor and 3% fifth-order harmonic distortion) at PCC is added, showing the operation of microgrid under distorted and unbalanced grid conditions. Moreover, unbalanced and nonlinear loads are also connected, illustrating performances under different load conditions. Diode rectifier is used to perform nonlinear loads.

• *Scenario I: synchronization criteria comparison*

In this case, $\Delta\mathbf{v}$ given respectively by synchronization criteria in Table I and the proposed *microgrid synchronization criteria* are applied at the instant of reconnection. The current responses are shown in Fig. 14. It can be observed that the envelopes and amplitudes of grid currents are consistent with Fig. 8, thus verifying the fundamental response analysis. In addition, it also indicates that if $\Delta\mathbf{v}$ meets the proposed *microgrid synchronization criteria*, a smooth transition can be achieved.
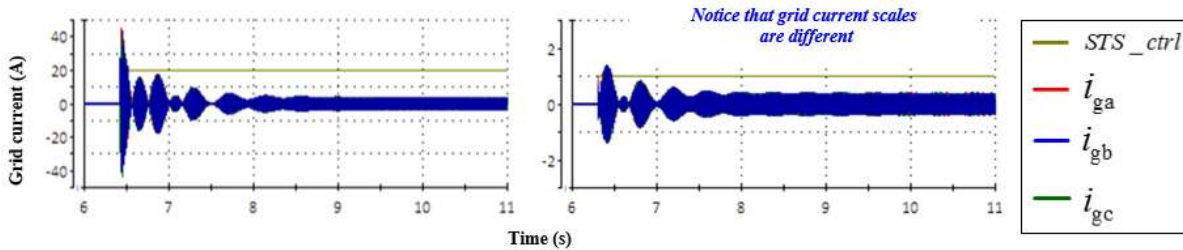
Fig. 14. Real-time HiL results in *Scenario I*. Left: synchronization criteria in Table I are applied; Right: proposed microgrid synchronization criteria are applied.
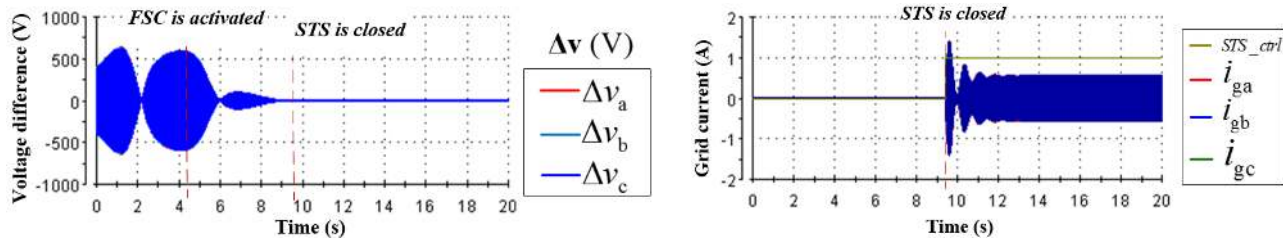

Fig. 15. Proposed FSC in *Scenario II*. Left: voltage difference; Right: grid current.
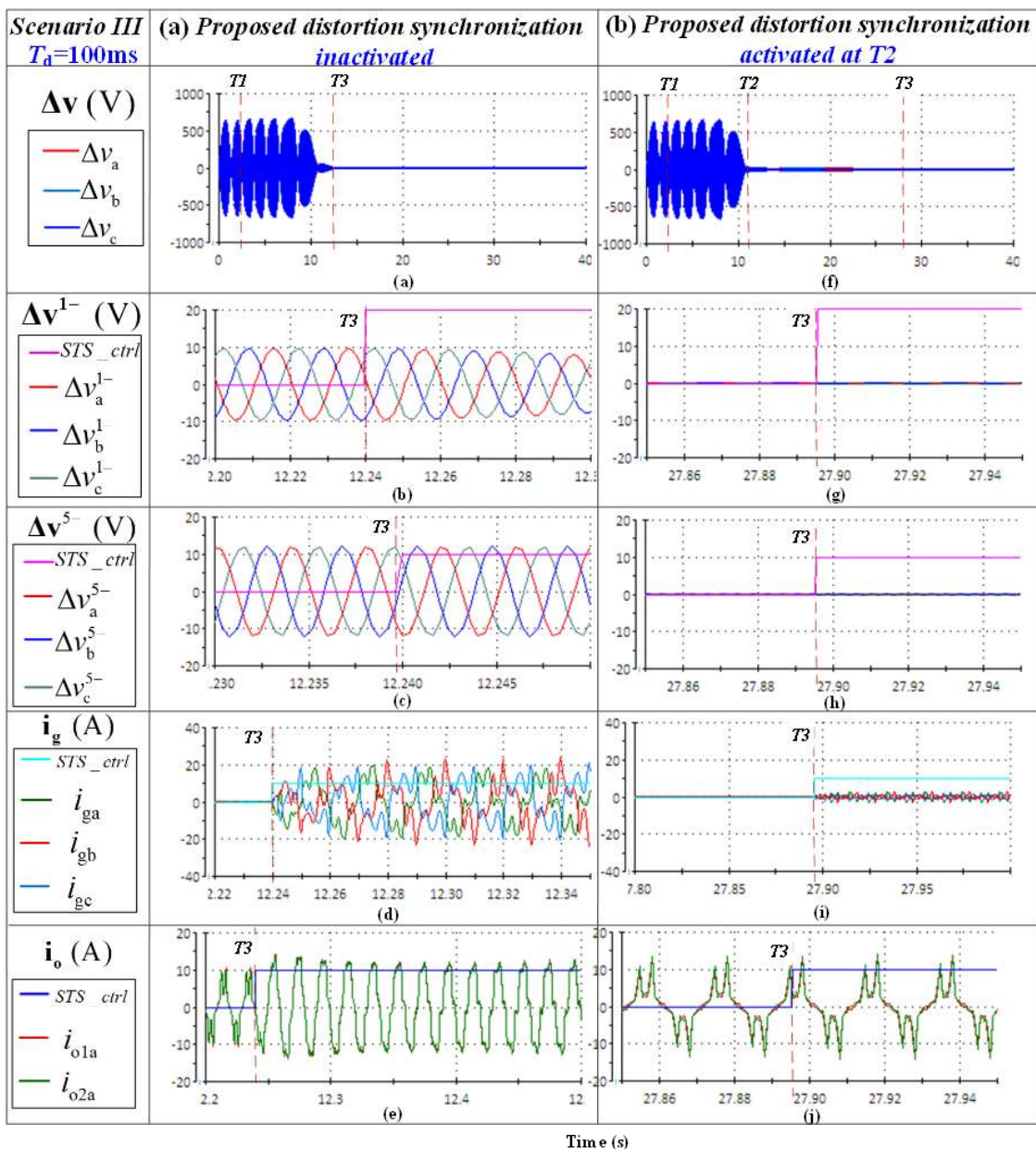

Fig. 16. Real-time HiL results in *Scenario III*. (a) ~ (e): *Scenario III (a)*; (f) ~ (j): *Scenario III (b)*.

TABLE III
VCM-VSC PARAMETERS

Parameters	Symbol	Value
Power stage parameters (VCM-VSC1 is 100% and VCM-VSC2 is 105%)		
Nominal output voltage	V_N	230V
Nominal output frequency	f_N	50Hz
Converter-side inductor	z_f	0.1 Ω, 1.8mH
Grid-side inductor	z_L	0.1 Ω, 1.8mH
Filter Capacitor	z_{cf}	1 Ω, 27μF
Secondary control parameters		
FSC	k_{pE}, k_{iE}	0.01, 1.5
	k_{pangle}, k_{iangle}	1.84, 1.7
DSC	k_{sp}^h, k_{si}^h	0.5, 1
Communication delay	T_d	100ms

- *Scenario II: proposed FSC*

In this case, only fundamental positive sequence voltage differences are applied during the reconnection process to verify FSC. The results are shown in Fig. 15. It can be seen that a fast and stable synchronization without relying on high-speed communication systems is achieved.

- *Scenario III: proposed active synchronization control*

Two cases are compared in this scenario: (a) without / (b) with the proposed DSC and distortion synchronization check block. The results are shown in Fig. 16. System operation process is given as follows.

At the beginning, the STS is off and microgrid operates in islanded mode. In this case, nonlinear loads and unbalanced loads as well as grid distortion are shown in Fig. 13. Microgrid voltage unbalance factor is 1.6% and fifth-order voltage distortion is 1%, while the grid unbalance factor is 2% and fifth-order 3%. The maximum fundamental and fifth-order negative sequence voltage differences are respectively around 10V and 12V as shown in Figs. 16(b) and (c).

At T1, proposed FSC is activated in *Scenario III* (a) and (b). After that, the synchronization of fundamental positive sequence voltages is started and instantaneous voltage difference is gradually decreased as shown in Figs. 16 (a) and (f).

At T2, proposed DSC is activated in *Scenario III* (b). After that, fundamental negative sequence and harmonic voltages can be synchronized and voltage differences are almost zero before closing the STS as shown in Figs. 16 (g) and (h). In *Scenario III* (a), no actions are applied. Therefore, voltage differences will be maintained until fundamental positive sequence voltages are synchronized and the STS is closed as shown in Figs. 16(b) and (c).

At T3, STS is closed in *Scenario III* (a) and (b). Due to no distortion synchronization check block, T3 occurs earlier in *Scenario III* (a) than (b). As shown in Figs. 16 (d) and (i), instantaneous grid currents are significantly reduced with the proposed synchronization control. In addition, there is little impact on the current-sharing as shown in Figs. 16 (e) and (j). Moreover, in *Scenario III* (b), $\mathbf{i_{o1}}$ and $\mathbf{i_{o2}}$ almost have no change during this period. Unbalanced and harmonic currents are still taken by VCM-VSC units rather than suddenly flow into the grid, which maybe aggravates power quality of the grid.

VI. CONCLUSION

The instant of microgrid reconnection to the main grid presents a transient response that can be divided into fundamental and harmonic responses. Based on the analysis of the transition between islanded and grid-connected modes, the minimization of fundamental and harmonic voltage differences is an effective way to achieve a smooth reconnection.

This paper proposes a distributed active synchronization strategy implemented in the secondary control level of a hierarchical control structure. The proposed approach can actively adjust the fundamental positive and negative sequence components as well as low order harmonic components of the microgrid so as to accurately track the main grid voltage. The paper shows that by using only local controllers in the primary control level this functionality cannot be achieved. The proposed method was tested under different grid and load conditions. Real-time HiL results show that the inrush current during the reconnection is effectively reduced, and a smooth transition is achieved by using the proposed synchronization scheme even under unbalanced and distorted voltage conditions

VII. REFERENCES

[1] *IEEE Guide for Design, Operation, and Integration of Distributed Resource Island Systems with Electric Power Systems*, IEEE Std 1547.4-2011, pp.1-54, July 20 2011.

[2] S.-H. Hu, C.-Y. Kuo, T.-L. Lee and J. M. Guerrero, "Droop Controlled Inverters with Seamless Transition between Islanding and Grid-Connected Operations", in *Proc. ECCE*, 2011, pp. 2196-2201.

[3] C. -W. Chang and Y. -R. Chang, "Energy storage systems for seamless mode transfer in microgrid," in *Proc. PEDS*, 2011, pp. 799–802.

[4] R. Majumder, A. Ghosh, G. Ledwich and F. Zare, "Control of parallel converters for load sharing with seamless transfer between grid connected and islanded modes," in *Proc. PESGM*, July 2008, pp.1-7.

[5] M. Rizo, F. Huerta, E. Bueno, and M. Liserre, "A synchronization technique for microgrid reclosing after islanding operation", in *Proc. IECON*, 2012, pp. 5596-5601.

[6] T. L. Vandoorn, B. Meersman, J. D. M. De Kooning, and L. Vandevelde, "Transition from islanded to grid-connected mode of microgrids with voltage-based droop control," *IEEE Transactions on Power Systems*, DOI: 10.1109/TPWRS.2012.2226481.

[7] Y. Li, D. M. Vilathgamuwa, and P. C. Loh, "Design, analysis, and real-time testing of a controller for multibus microgrid system," *IEEE Trans. Power Electron.*, vol. 19, no. 5, pp. 1195–1204, Sep. 2004.

[8] Y. Q Jia, D. K. Liu, and J. Liu, "A novel seamless transfer method for a microgrid based on droop characteristic adjustment," in *Proc. IPEMC*, 2012, pp. 362-367.

[9] C. Jin, M. Z. Gao, X. f. Lv and M. Chen, "A seamless transfer strategy of islanded and grid-connected mode switching for microgrid based on droop control," in *Proc. ECCE*, 2012, pp. 969 – 973.

[10] Chia-Tse Lee, Ruei-Pei Jiang, and Po-Tai Cheng, "A Grid Synchronization Method for Droop-Controlled Distributed Energy Resource Converters," *IEEE Trans. Ind. Appl.*, vol. 49, no. 2, pp. 954 – 962, 2013.

[11] T. M. L. Assis and G. N. Taranto, "Automatic Reconnection From Intentional Islanding Based on Remote Sensing of Voltage and Frequency Signals," *IEEE Trans. Smart Grid*, vol. 3, no. 4, pp. 1877 – 1884, Sep. 2012.

[12] C. Cho, J-Hong Jeon, J-Yul Kim, S. Kwon, K. Park, and S. Kim "Active synchronizing control of a microgrid," *IEEE Trans. power. Electron*, vol. 26, no. 12, 2009, pp. 3707–3719.

[13] J. C. Vasquez, J. M. Guerrero, M. Savaghebi, E. G. Carrasco, and R. Teodorescu, "Modeling, analysis, and design of stationary reference frame droop controlled parallel three-phase voltage source inverters." *IEEE Trans. Ind. Electron.*, vol. 60, no. 4, 2013, pp. 1271–1280.

[14] H. Laaksonen and K. Kauhaniemi, "Synchronized reconnection of island operated LV microgrid back to utility grid," in *Proc. ISGT Europe*, 2010, pp. 1- 8.

[15] J. M. Guerrero, J. C. Vasquez, J. Matas, L. G. Vicuna, and M. Castilla, "Hierarchical control of droop-controlled DC and AC microgrids—a general approach towards standardization," *IEEE Trans. Ind. Electron.*, vol. 58, no. 1, pp. 158-172, Jan. 2011.

[16] M. Savaghebi, A. Jalilian, J. C. Vasquez, and J. M. Guerrero, "Secondary control for voltage quality enhancement in microgrids," *IEEE Trans. Smart Grid*, vol. 3, no. 4, pp. 1893–1902, Dec. 2012.

[17] F. Katiraei, R. Iravani, N. Hatziargyriou, and A. Dimeas, "Microgrids management-controls and operation aspects of microgrids," *IEEE Power Energy Mag.*, vol. 6, no. 3, pp. 54–65, May/Jun. 2008.

[18] F. B. del Blanco, M. W. Degner, and R. D. Lorenz, "Dynamic analysis of current regulators for AC motors using complex vectors," *IEEE Trans. on Ind. Appl.*, vol. 35, no. 6, pp. 1424-1432, 1999.

[19] K. Dai, P. G. Liu, J. Xiong, and J. Chen, "Comparative study on current control for three phase SVPWM voltage source converter in synchronous rotating frame using complex vector method," in Proc. PESC, 2003, pp. 695-700.

[20] M. Savaghebi, J.C. Vasquez, A. Jalilian, J.M. Guerrero, Tzung-Lin Lee, "Selective harmonic virtual impedance for voltage source inverters with LCL filter in microgrids," Energy Conversion Congress and Exposition (ECCE), pp.1960-1965, 15-20 Sept. 2012.

[21] *IEEE Standard for Interconnecting Distributed Resources With Electric Power Systems*, IEEE Std 1547-2003, 2003: 0_1- 16.

[22] R. C. Dugan, M. F. McGranaghan, S. Santoso, and H. W. Beaty, *Electrical Power Systems Quality*. 2nd ed., New York: McGrawHill, 2003.

[23] *IEEE Recommended Practice and Requirements for Harmonic Control in Electric Power Systems*, IEEE Standard 519-1992, 1992.

[24] A. Baggini. *Handbook of power quality*, John Wiley & Sons, 2008.

[25] *Power quality–Three-phase voltage unbalance*, GB/T 15543-2008, 2008.

[26] K. Lee. *Power Quality Analysis and New Harmonic and Unbalance Control of Modern Adjustable Speed Drives Or Uninterruptible Power Systems Under Nonideal Operating Conditions*. BiblioLife, LLC, 2011.

[27] P. Mattavelli, "A closed-loop selective harmonic compensation for active filters," *IEEE Trans. Ind. Appl.*, vol.37, no.1, pp. 81 - 89, 2001.

[28] P. Mattavelli, "Synchronous-frame harmonic control for high-performance AC power supplies," *IEEE Trans. Ind. Appl.,* vol.37, no.3, pp. 864-872, 2001.

[29] S. Chung, "A phase tracking system for three phase utility interface inverters," *IEEE Trans. Power Electron.*, vol. 15, May 2000, pp. 431-438.